International Journal of Heat and Fluid Flow 31 (2010) 450–459

Contents lists available at ScienceDirect

International Journal of Heat and Fluid Flow

journal homepage: www.elsevier.com/locate/ijhff

Transient dynamics of the flow around a NACA 0015 airfoil using fluidic vortex generators

W.L. Siauw [b], J.-P. Bonnet [a,*], J. Tensi [b], L. Cordier [a], B.R. Noack [a], L. Cattafesta [c]

[a] Institut Pprime, CNRS – Université de Poitiers – ENSMA, UPR 3346, Département Fluides, Thermique, Combustion, CEAT, 43 rue de l'Aérodrome, F-86036 Poitiers Cedex, France
[b] Institut Pprime, CNRS – Université de Poitiers – ENSMA, UPR 3346, Département Fluides, Thermique, Combustion, ENSMA - Téléport 2, 1 Avenue Clément Ader, BP 40109, F-86961 Futuroscope Chasseneuil Cedex, France
[c] Florida Center for Advanced Aero-Propulsion (FCAAP), Department of Mechanical and Aerospace Engineering, University of Florida, 231 MAE-A, Gainesville, FL 32611, USA

A R T I C L E   I N F O

Article history:
Received 18 August 2009
Received in revised form 24 February 2010
Accepted 25 February 2010
Available online 19 March 2010

Keywords:
Flow control
NACA airfoil
Vortex generators
Transient processes
Proper Orthogonal Decomposition
Reduced-order model

A B S T R A C T

The unsteady activation or deactivation of fluidic vortex generators on a NACA 0015 airfoil is studied to understand the transient dynamics of flow separation control. The Reynolds number is high enough and the boundary layer is tripped, so the boundary layer is fully turbulent prior to separation. Conditional PIV of the airfoil wake is obtained phase-locked to the actuator trigger signal, allowing reconstruction of the transient processes. When the actuators are impulsively turned on, the velocity field in the near wake exhibit a complex transient behavior associated with the formation and shedding of a starting vortex. When actuation is stopped, a more gradual process of the separation dynamics is found. These results are in agreement with those found in the literature in comparable configurations. Proper Orthogonal Decomposition of phase-locked velocity fields reveals low-dimensional transient dynamics for the attachment and separation processes, with 98% of the fluctuation energy captured by the first four modes. The behavior is quantitatively well captured by a four-dimensional dynamical system with the corresponding mode amplitudes. Analysis of the first temporal POD modes accurately determines typical time scales for attachment and separation processes to be respectively $t^+ = 10$ and 20 in conventional non-dimensional values. This study adds to experimental investigations of this scale with essential insight for the targeted closed-loop control.

1. Introduction

Suppressing or delaying flow separation over an airfoil at high incidence has been the subject of many studies for more than a century (Greenblatt and Wygnanski, 2000). Many different type of actuators can be used but, in this paper, we are specifically concerned by active control of flow separation via fluidic actuators. Most research focuses on open-loop pre-determined control using steady/unsteady jets without consideration of the state of the flow field. Examples of steady jet control techniques can be found in the work of Eldredge and Bons (2004), Sondergaard et al. (2002), Erm (2001), and Johnston and Compton (1992). In the case of unsteady jet actuation, readers are referred to, for example, Hansen and Bons (2006), Seifert et al. (2004), and Amitay and Glezer (2002b). In majority, these studies target the steady or quasi-steady state performance of lift enhancement and drag reduction at relatively low chord Reynolds number (typically <0.5 million). Closed-loop airfoil separation control has been studied at relatively low Reynolds number by Tian et al. (2006) and Pinier et al. (2007), and on a generic separated configuration at a chord Reynolds number of 16 million by Allan et al. (2000). Detailed studies concerning the transient process of flow attachment and separation in response to a synthetic jet actuator have been performed by Darabi and Wygnanski (2004a,b), and Amitay and Glezer (2002a, 2006). More recently, Mathis et al. (2009) performed a similar study using this time a steady jet to provoke separation for enhancement of mixing. Table 1 shows that the typical time scales that can be found in the literature for characterizing the attachment and separation processes are quite different. In this table, the time denoted with a + superscript is given in conventional non-dimensional values, *i.e.* non-dimensionalized by the length of the separation zone L_{sep} and the external velocity U_∞. In addition, it should be emphasized that, for the two first configurations, the flow is naturally separated and the actuation enforces flow attachment, whereas in Mathis et al. (2009), the flow is naturally attached and then the actuators promote separation.

So far, relatively little attention has been paid to the transient aspects of the problem. However, this aspect is fundamental in closed-loop control since the knowledge of the typical time scales

* Corresponding author.
E-mail addresses: Jean-Paul.Bonnet@univ-poitiers.fr (J.-P. Bonnet), Jean.Tensi@lea.univ-poitiers.fr (J. Tensi), Laurent.Cordier@univ-poitiers.fr (L. Cordier), Bernd.Noack@univ-poitiers.fr (B.R. Noack), cattafes@ufl.edu (L. Cattafesta).

0142-727X/$ - see front matter
doi:10.1016/j.ijheatfluidflow.2010.02.028

Table 1
Typical separation/attachment time scales. In the definition of the momentum coefficient C_μ, ρ_j is the actuator flow density, U_j denotes peak jet velocity, S_j is the total area of the actuators, ρ_∞ and U_∞ are the free stream density and free stream velocity respectively and, S_{ref} is usually taken as the length of the body under consideration (e.g. chord, or flap length) for two-dimensional configuration or total wing area for three-dimensional configuration.

Authors	Amitay and Glezer (2002a)	Darabi and Wygnanski (2004a)	Mathis et al. (2009)
Test configuration	Modified wing profile	Generic flap	Beveled splitter plate
Reynolds number	3.1×10^5 (scaled by wing chord and free stream velocity)	1.24×10^5 (scaled by flap length and free stream velocity)	1.44×10^5 (scaled by bevel length and free stream velocity)
Actuator type	Synthetic jet	Synthetic jet	Steady jet
$C_\mu = \frac{\rho_j U_j^2 S_j}{\frac{1}{2}\rho_\infty U_\infty^2 S_{\mathrm{ref}}}$	3.5×10^{-3}	5×10^{-4} to 8×10^{-4}	9×10^{-2} to 2.2×10^{-2}
t^+ (attachment)	$\sim$9.5	16–70 (16 is the optimal value)	5
t^+ (separation)	$\sim$14	20	25

and the associated dynamical behavior of the entire process are mandatory to act correctly on the flow. From the three examples mentioned above, it appears that no universal value exists for the attachment and separation length scales. These discrepancies can be attributed to several factors. First, the physics of the processes of separation and attachment are entirely dependent on whether the initial state is attached or separated. Second, the method of actuation is generally different for every study. However, the transient separation process may not depend on the specific characteristics of individual actuators or actuation techniques. Thirdly, the type of flow configuration (wing, flap or bevel) and the effects of Reynolds number cannot be neglected, especially at low Reynolds numbers (Seifert et al., 2004). Lastly, it should be emphasized that the determination of the typical time scales is not straightforward and can correspond to different definitions. One of the least-biased definition of unsteady separation points has been provided by Haller (2004), where distributed pressure and skin-friction measurements along the wall are used for this purpose. Here, since the main focus is on the modeling of the wake dynamics, we will estimate the time scales of the separation and attachment processes from the first temporal modes calculated from the POD of conditional averaged PIV data.

Reduced-order modeling is a vital enabler for developing closed-loop control strategies (Collis et al., 2004). Indeed, since the final objective is to perform real-time flow control of fully turbulent flows, methods to enable reductions of the dimension and complexity of the original problems are first necessary. In control theory, a standard approach is to determine the transfer function of the plant by system identification. It was used successfully in Rapoport et al. (2003), where closed-loop control were applied for vectoring by periodic excitation a turbulent jet. In turbulence, a tool generally used for model reduction is the Proper Orthogonal Decomposition or POD (Lumley, 1967). Another advantage of POD is the possibility of deriving a dynamical system that accurately represents the flow dynamics and that contains an actuation input explicitly. This POD reduced-order model (POD ROM) can then be used as a plant to determine an optimal (in a given sense) control law (see Bergmann and Cordier, 2008, for an example). In practice, the difficulty comes from the experiments, where despite the significant progress made in the measurement techniques, determining a POD ROM remains a challenging task. For illustration, Ausseur et al. (2006b) and Perret et al. (2006) succeeded in identifying POD-based ROM with experimental data but only for uncontrolled configurations. In short, the identification procedures consist of estimating the coefficients of the dynamical system such that the reduced-order model reproduces correctly the original actuated dynamics. A summary of these calibration algorithms can be found in a recent paper (Cordier et al., 2010), where the main different algorithms are exemplified for the wake flow behind a circular cylinder. Depending on the phenomenological behavior of the flow, the dynamical systems can be first- or higher-order (Ausseur et al., 2006b). Hereafter, the two-point velocity correlation tensor has been used as kernel for the POD. This is the common choice in the literature (Cordier and Bergmann, 2008a) but other kernels can be used, such as correlation of vorticity (Kostas et al., 2005), or correlation of the non-linear convection term in the Navier–Stokes equations (Ausseur et al., 2006a). Moreover, for design of the control system, real-time estimation of the states is required. This is currently provided in experiments using linear stochastic estimation (LSE). Essentially, with LSE, the statistical information contained in the two-point correlation tensor is combined with instantaneous information to estimate other fields (Adrian, 1996). Recently, a pressure sensor array has been used to estimate flow fields by Pinier et al. (2007). Similarly, Stalnov et al. (2007) used signals from a surface mounted hot-film array to estimate the structures in the wake of a D-shaped profile. In summary, POD reduced-order modeling and LSE could form the basis of a control strategy for closed-loop separation control.

The current study concerns the transient dynamics of attachment and separation over a NACA 0015 airfoil operating at a chord Reynolds number of about 1 million in response to the deployment and removal of an array of 44 steady pitched (30°) and skewed (60°) fluidic vortex generators (FVGs) positioned at 30% of the chord length c of the airfoil (see Fig. 1). The Reynolds number is supposed sufficiently high to do not have significant effects on the flow. The chosen flow condition is such that jet deployment corresponds to complete flow attachment over the airfoil; jet removal will cause flow separation up to an extent defined by the uncontrolled separated state. This paper utilizes conditional PIV to probe the transient flow dynamics. In particular, the FVGs are pulsed at a frequency of 1 Hz in an "on–off" manner in order to enable conditional sampling for both experiments involving PIV and hot wire anemometry. The objective of the current work is to provide a description of the physics of flow attachment and separation in response to the deployment and removal of the FVGs. Focus is placed on POD reduced-order modeling based on conditionally averaged PIV data.

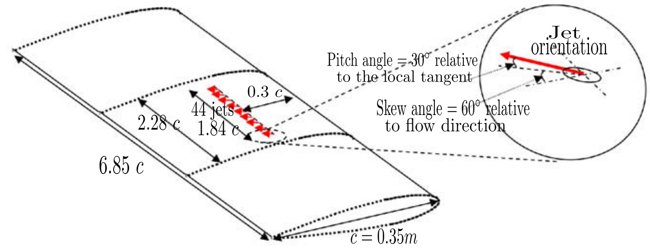

Fig. 1. FVGs installed at 30% of chord length.

This manuscript is organized as follows. Section 2 presents the flow configuration, the experimental set-up of the PIV measurements, and the processing which has been performed. Section 3 introduces the reduced-order model used for identifying the natural and actuated transient dynamics of the airfoil wake. Section 4 begins with a brief presentation of the results of the phase-averaging for the jet deployment and jet removal processes. For these transient flows, a POD analysis of the ensemble-averaged PIV data is presented in Section 4.2. This includes: (i) a POD analysis of the flow dynamics, (ii) an identification of a POD ROM for the actuated flow and (iii) an estimation of the time scales of flow attachment and separation from the temporal POD modes.

2. Experimental set-up and data analysis

2.1. Flow configuration and measurements

The closed-loop wind tunnel used for the study had a test section size of 2.4 m (width) by 2.6 m (height) by 6 m (length). The turbulence level is 0.5% at $U_\infty = 40$ m/s. A 0.35 m chord, 2.4 m span NACA 0015 airfoil model was installed in the test section. To trip the boundary layer, different sizes of roughness were considered in Siauw (2008). Finally, a carborandum grit of 80 μm was applied at 0.4% of the chord from the leading edge of the airfoil which is before the laminar separation bubble. The test condition corresponded to a chord Reynolds number of approximately 1 million. Fluidic vortex generators were deployed through an array of holes located at 30% chord of 44×1 mm diameter orifices, spaced 15 mm apart in the spanwise direction. This array occupied the central one third spanwise portion of the airfoil. As shown in Fig. 1, the FVGs were pitched 30° and yawed at 60°. The peak velocity of the jets was set at about 200 m/s, corresponding to a C_μ of 0.67%. The dynamics of the jets is fully quantified in Siauw (2008) (see Chapter 4). The influence of the incidence angle on the separation was carefully analyzed in Siauw (2008). It was found that at 11° of incidence the separation was two-dimensional with minimal vibration, thus giving a suitable and stable test condition for reduced-order modeling. In addition, $L_{sep} = 0.3c$ for this value of incidence.

To characterize the transients, the FVGs deployment system must respond much faster than the characteristic times of attachment and separation. This was achieved by installing four ASCO solenoid valves (CM25-5W) inside the airfoil model, such that 11 orifices were controlled by each valve. These valves were capable of an average response time (time to open/close the valve) of about 3 ms (Siauw, 2008). The valves were operated by controlling the on/off state of a relay that was triggered via a square wave signal. To ensure fast circuit response, a solid state electronic type was chosen for the relay. A LaVision PIV system was used to study the transient dynamics of the wake (see Fig. 2) in response to flow attachment and separation over the NACA 0015 airfoil via deployment and deactivation of the FVGs, respectively. The system software synchronized laser pulsing and image acquisition from a camera system with a resolution of 1350 by 1048 pixels using the valve external trigger signal (1 Hz) for conditional sampling. A laser pulsed with a time interval of 200 μs was used. The two images, captured during the laser pulses, were cross correlated successively starting from an interrogation window size of 64 by 64 pixels to a final size of 16 by 16 pixels with a 50% overlap ratio. The uncertainty of the PIV measurements can be estimated from pure statistics (Bendat and Piersol, 1971) or taking into account the specificities of the PIV method, including the data processing method (Stanislas et al., 2008). In the present experiments, the resulting uncertainty based on second-moment statistics is estimated to be of the order of 6%.

2.2. Post-processing

Starting with nomenclature, points of the experimental domain are described in a Cartesian coordinate system, $\boldsymbol{x} = (x, y)$, where the x–axis is aligned with the flow and the y–axis with the transverse direction (see Fig. 2). Similarly, the velocity field is denoted by $\boldsymbol{u} = (u, v)$, where u and v are components aligned with the x– and y–direction. Following Reynolds and Hussain (1972), the flow manipulated by time periodic on–off forcing can be written as:

$$\boldsymbol{u}(\boldsymbol{x}, t) = \bar{\boldsymbol{u}}(\boldsymbol{x}) + \tilde{\boldsymbol{u}}(\boldsymbol{x}, t) + \boldsymbol{u}'(\boldsymbol{x}, t), \tag{1}$$

where $\bar{\boldsymbol{u}}$ is the time-independent mean flow, $\tilde{\boldsymbol{u}}$ is the quasi periodic fluctuating component, $\boldsymbol{u}'$ is the random fluctuating component, and t represents time. The phase-averaged velocity is defined as

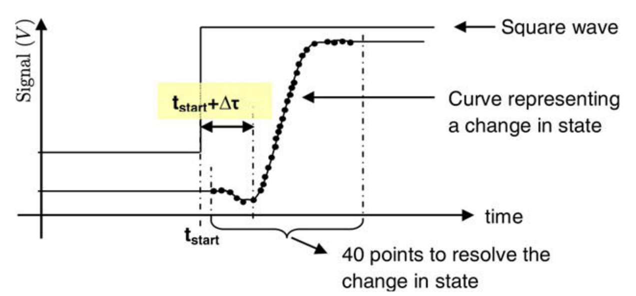

Fig. 3. Illustration of conditional PIV sampling to characterize the change of flow state after FVGs deployment. A similar figure can be drawn for the removal of the FVGs with t_{start} corresponding this time to the end of the trigger signal.

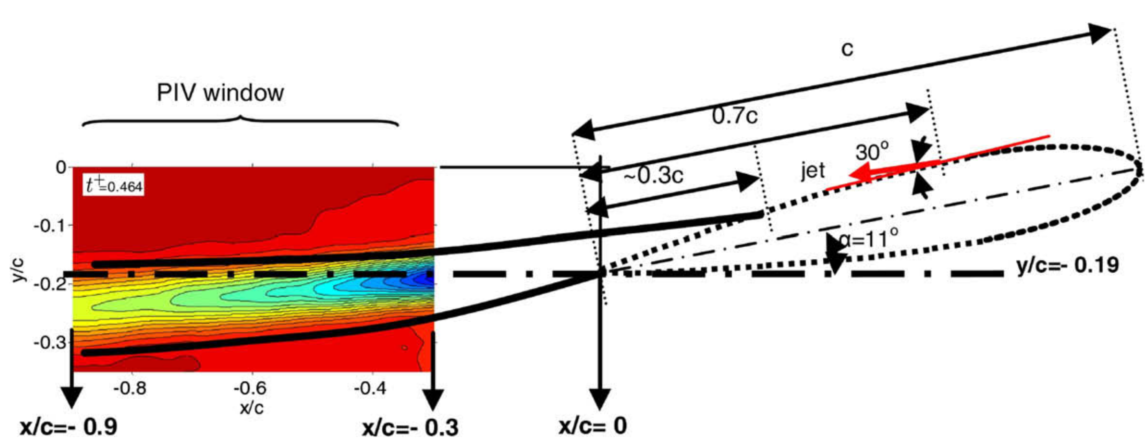

Fig. 2. Schematic of the PIV window in the airfoil wake. The incidence angle is fixed at 11°.

$$\langle \boldsymbol{u}(\boldsymbol{x},t)\rangle \triangleq \bar{\boldsymbol{u}}(\boldsymbol{x}) + \tilde{\boldsymbol{u}}(\boldsymbol{x},t), \tag{2}$$

$$\triangleq \frac{1}{N_{\text{cycles}}} \sum_{n=0}^{N_{\text{cycles}}-1} \boldsymbol{u}(\boldsymbol{x}, t + nT_{\lozenge}), \tag{3}$$

where $T_{\lozenge}$ is the phase period, and N_{cycles} is the number of cycles used in the phase average.

Fig. 3 illustrates the conditional sampling technique employed during FVGs deployment. In the current study, $T_{\lozenge} = T_{\text{cj}}$, where T_{cj}, the period of the square wave signal used to trigger the control valves, was chosen to be sufficiently long for the flow to reach an asymptotic steady state (Siauw, 2008). Moreover, in our case, 300 cycles were found sufficient (Siauw, 2008) to obtain converged ensemble-averaged statistics. A total of $N_\tau = 40$ time delays have been used to resolve the change in flow structure in the wake due to flow attachment or separation over the airfoil. Therefore, the time t is discretized as

$$t_j = t_{\text{start}} + \tau_j \quad \text{with} \quad j = 1, \ldots, N_\tau,$$

where for FVGs deployment, t_{start} corresponds to the start of the trigger signal, whereas, for the FVGs removal, t_{start} corresponds to the end of the trigger signal.

Important information about the transient dynamics can be retrieved at each time delay by analyzing the ensemble-averaged statistics of the 300 independent snapshots for each time delay. Conditional POD can be applied to this data set according to:

$$\langle \boldsymbol{u}(\boldsymbol{x},t_j)\rangle = \langle \boldsymbol{u}(\boldsymbol{x},t_1)\rangle + \sum_{n=1}^{N_\tau=40} a_n(t_j)\boldsymbol{u}_n(\boldsymbol{x}) \quad \text{with} \quad j = 1, \ldots, N_\tau, \tag{4}$$

where $a_n(t_j)$ and $\boldsymbol{u}_n(\boldsymbol{x})$ correspond respectively to the temporal and spatial POD eigenfunctions. A dynamical system that describes the uncontrolled or controlled flow can be deduced by projecting the Navier–Stokes equations onto the POD modes via the Galerkin approach (Holmes et al., 1997; Cordier and Bergmann, 2008b). However, it is difficult to construct a reduced-order model describing the flow transients during an experiment. Indeed, the control input is in general not explicitly included in the POD expansion (4) unless using some specific approaches such as the control function method (Bergmann et al., 2005). An alternative is an identified forcing term for the actuation effect in the Galerkin system (Luchtenburg et al., 2009).

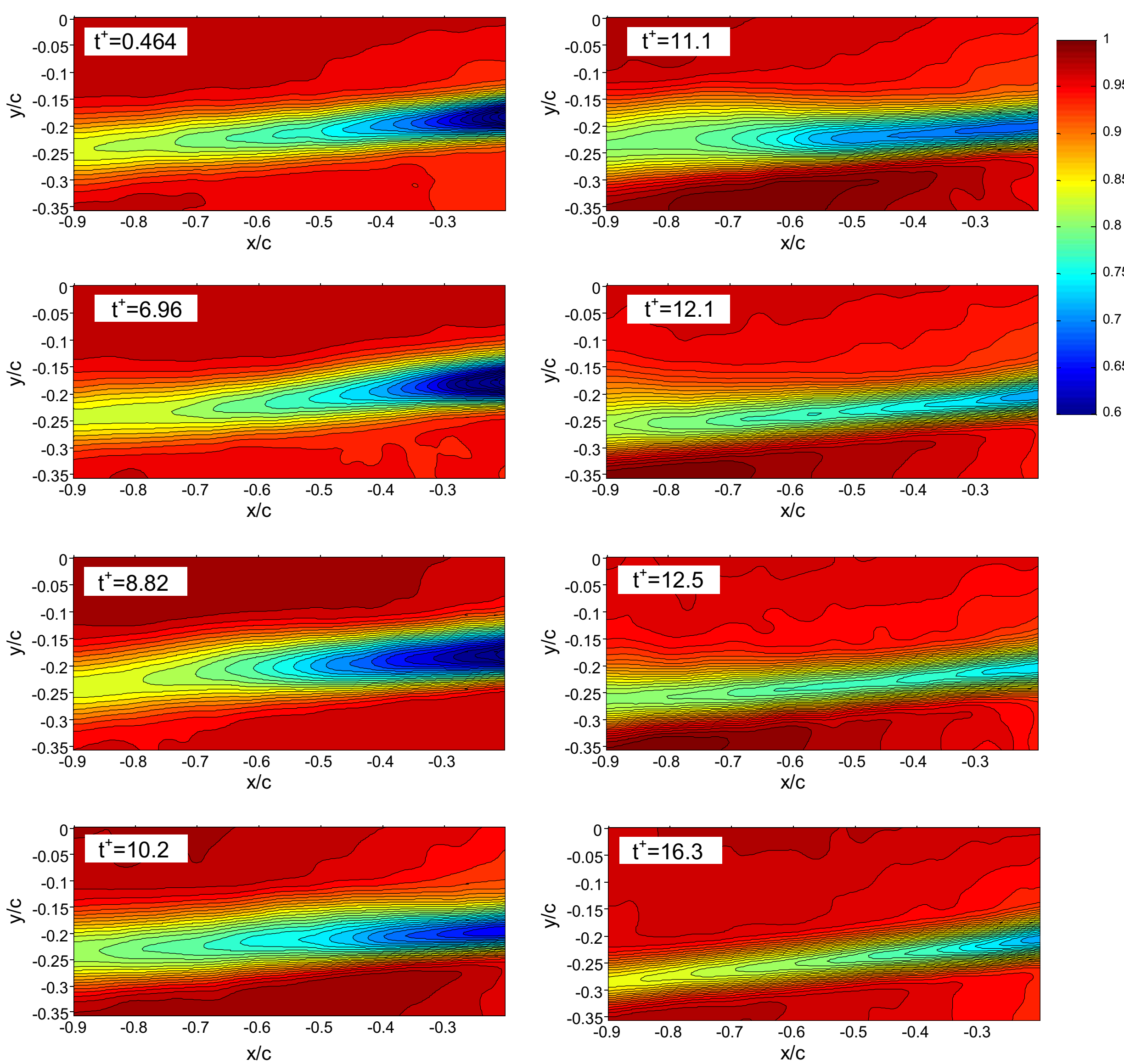

Fig. 4. Evolution of the ensemble-averaged mean streamwise velocity ($\langle u\rangle/U_\infty$) in the airfoil wake during the attachment process.

3. ROM of conditional averaged data

In practice, the use of the control function method (Bergmann et al., 2005) has two drawbacks. Firstly, it is necessary to determine specifically one or more actuation modes. Secondly, the POD ROM is then non-linear and it is thus impossible to use directly the tools of linear control (Burl, 1999, for instance). Thirdly, the ensemble-averaging procedure expressly removes the driving fluctuations which act on the base flow transients as Reynolds stresses (Tadmor et al., in press). For these reasons, we will identify a dynamical system from PIV data. We postulate the most simple system structure consistent with phenomenology *i.e.* a stable linear time-invariant natural base flow dynamics with a linear forcing term:

$$\frac{da_i(t)}{dt} = \sum_{j=1}^{N_{gal}} A_{ij}\ a_j(t) + B_i\ b(t), \tag{5}$$

where N_{gal} is the number of POD modes conserved in the model. A good choice for the value of N_{gal} can be based on the POD convergence (see Fig. 9). In (5), A_{ij} and B_i are the coefficients associated with the temporal modes and suitably scaled control command, respectively. For $b(t)$, several choices are possible: command signal of the solenoid valves, velocity measurements of the FVG, ...In the current work, $b(t)$ is approximated by the velocity fluctuations from a hotwire positioned 3 mm from an FVG orifice with the tunnel operating. Indeed, it was shown in Siauw, 2008 that the time evolutions of the hotwire signal and of the square wave signal used to trigger the control valves are in very good agreement. Then, employing one in place of the other does not have any significant influence. For determining the coefficients A_{ij} and B_i from the known $a_j(t)$ and $b(t)$, standard identification methods have been applied (Cordier et al., 2010). Rigorously, the domain of validity of the model is then restricted to the range of parameters used for the identification (same values of free stream velocity and angle of incidence, in particular). However, we have good reasons to believe that the qualitative behavior (forced damped linear system) remains the same for a large class of pre-stall parameters. Once the linear coefficients (A_{ij} and B_i) are determined, we can simulate the system dynamics by integrating (5) in time. A 5th order Runge–Kutta integration scheme was used for numerical integration. Such a model is useful as an exploratory test-bed to study the transient dynamics if there are changes to the initial condition and actuation signal.

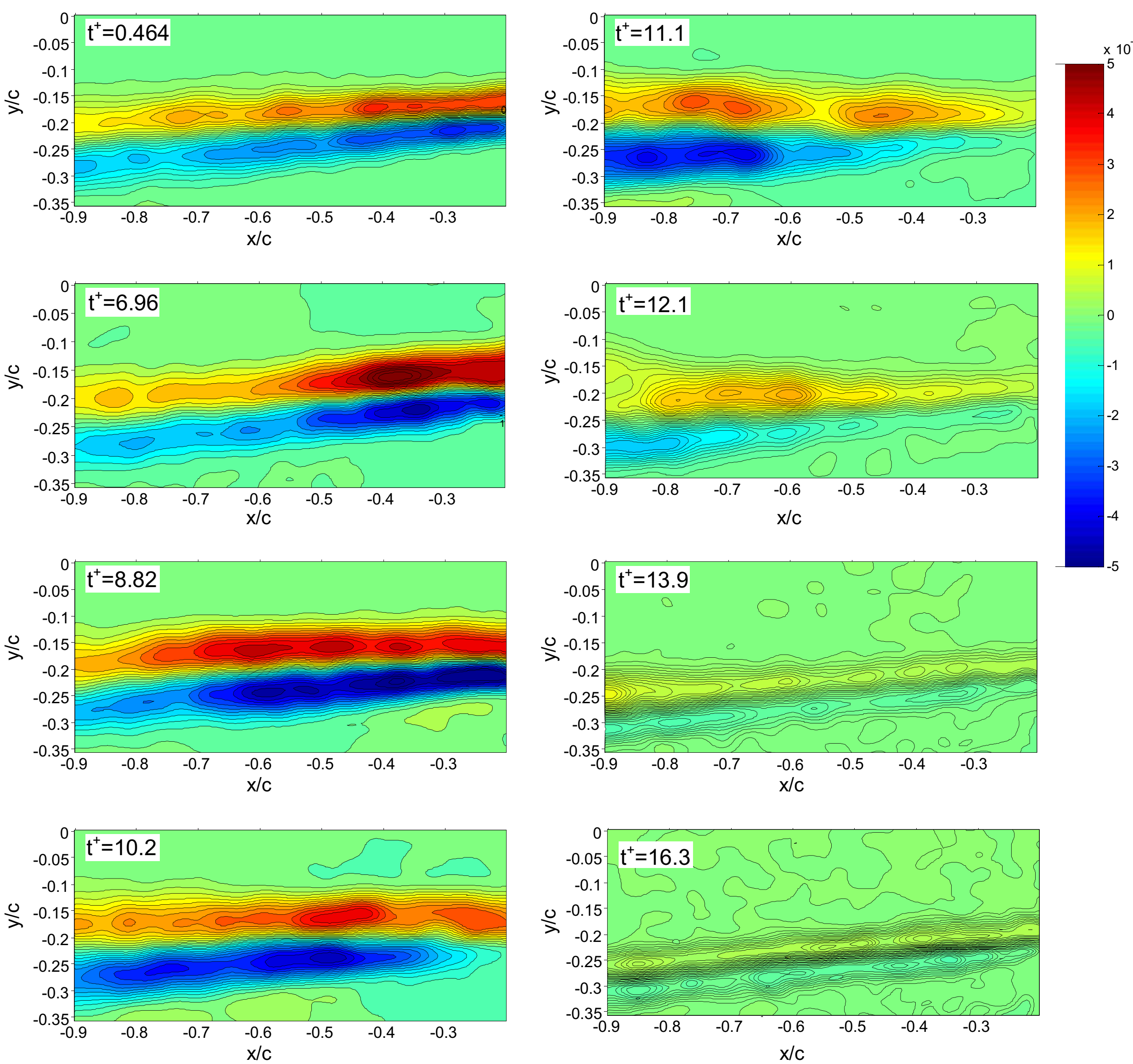

Fig. 5. Evolution of the ensemble-averaged turbulent shear stress ($\langle u'v'\rangle/U_\infty^2$) in the airfoil wake during the attachment process.

4. Unsteady behaviour

4.1. Changes in mean and turbulent velocity fields

The conditional averaging process allows for the analysis of the time evolution of the wake. This time evolution is obtained from (3).

4.1.1. Attachment phase

When the FVGs are deployed, it can be observed from the contours of $\langle u\rangle/U_\infty$ velocity plotted in Fig. 4 that the wake starts to undulate between $t^+ = 6.96$ and 8.82. This first phase of dynamics is not characterized by an increase in the width of the wake. The wake starts to widen from $t^+ = 8.82$ to $t^+ = 10.2$; this increase is rapid and progresses from the upstream to downstream position. This interval corresponds to the initial increase of drag associated with the "starting vortex" passage observed by several authors (e.g., Amitay and Glezer, 2002a). From $t^+ = 10.7$ to 13.5 (see Siauw (2008), for more time instants than those presented in Fig. 4), the wake reduces in size progressively from upstream to downstream. Thereafter, the wake tends asymptotically to the final reduced width. During the whole process, the velocity in the region of the wake axis has been redistributed such that the initially higher velocity deficit at $x/c = -0.3$ is reduced (*i.e.* higher velocity) and, conversely, the initially lower velocity deficit at $x/c = -0.9$ is increased (*i.e.* lower velocity). The estimated drag coefficients, determined from hot wire measurements, are consistent with the observation of increase in wake width (increase in C_d) followed by a decrease in width (decrease in C_d). The transient phenomenon is also related to the complex turbulence behavior depicted in Fig. 5, in which the shear stress $\langle u'v'\rangle$ contours are plotted. The shear stress is more intense in the upstream position at $t^+ = 0.464$ (*i.e.*, before the effects of the jet deployment is felt). From $t^+ = 6.96$ to 8.82, the shear stresses increase in intensity in the downstream direction. At $t^+ = 10.2$, the high shear stress region begins to decrease from the upstream direction. The negative shear stress region (wake bottom) has been evacuated from the PIV window more quickly than the positive shear stress regions (wake top); this occurs from $t^+ = 11.1$ to 13.9. Finally, if we consider the shear stress profiles in the normal direction at $x/c = -0.85$, it can be shown (Siauw, 2008) that, relative to the value at $t^+ = 0.464$, the shear stress increases by more than 50% during the transient and decreases by about 50 attached over the airfoil.

4.1.2. Separation phase

When the FVGs are deactivated, the flow starts to separate and returns to its baseline condition. The mean streamwise velocity contours are plotted in Fig. 6. The velocity field shows a gradual enlargement of the wake and an upward shift of the wake axis, which is similar to what was encountered for the jet activation process. However, the undulation (wave like behaviour) observed in the attachment phase is no longer present in the wake. Thus, the passage of large eddies with spatial scales larger than that of the uncontrolled vortex street in the downstream direction is probably not present. This statement is substantiated in the analysis of the turbulent shear stress plotted in Fig. 7. The axis of the wake can be determined by the line of zero shear at the interface of the positive upper and negative lower regions. Unlike the case of jet

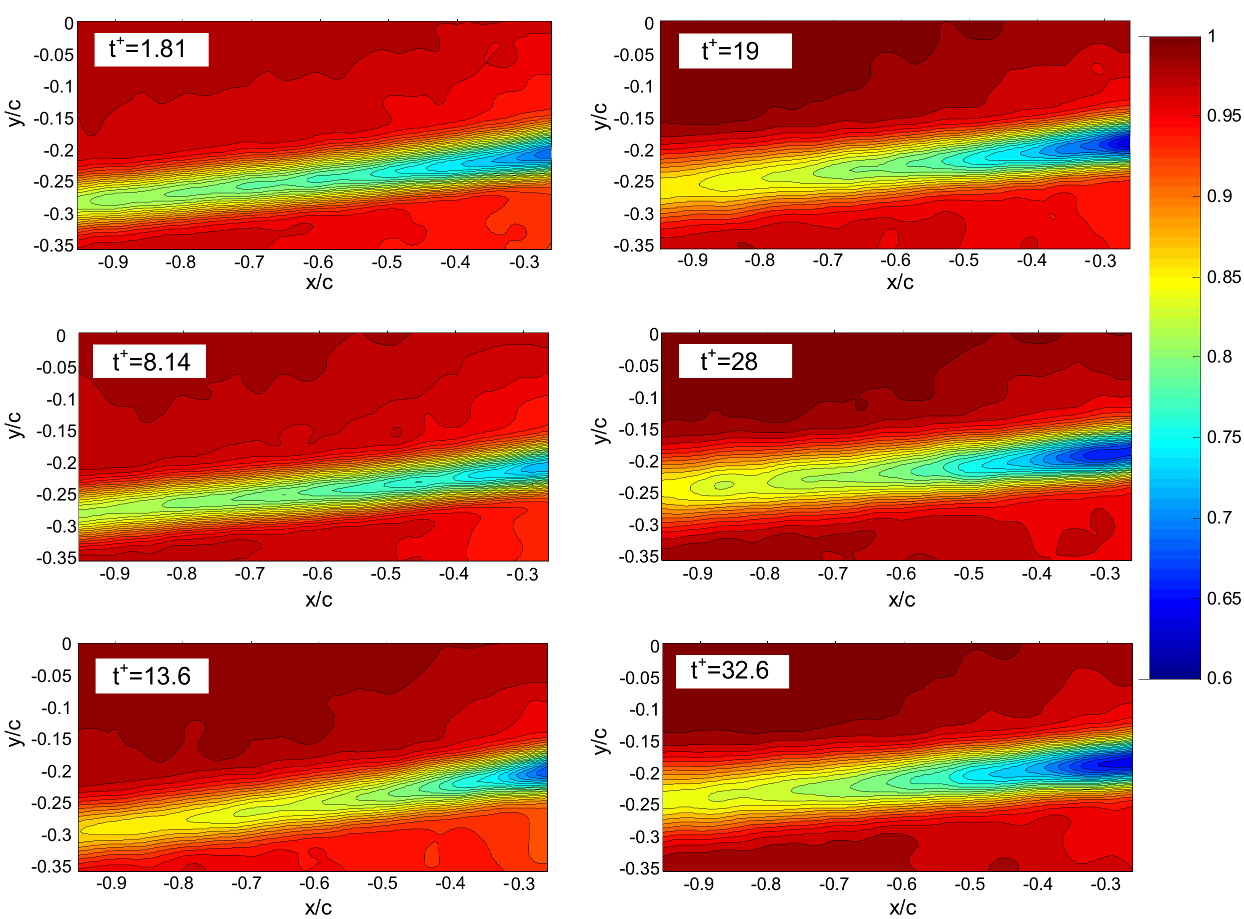

Fig. 6. Evolution of the ensemble-averaged mean streamwise velocity ($\langle u\rangle/U_\infty$) in the airfoil wake during the separation process.

deployment (see Fig. 5), undulation in the line of zero shear is observed during the transient. Based on the contour levels along the wake axis (Siauw, 2008), the velocity deficit decreases at the downstream position at $x/c = -0.85$. The inverse is observed at the upstream position at $x/c = -0.3$. The movement of the wake axis proceeds by a slight downward movement followed by a gradual upward movement towards its asymptotic position. The estimated drag coefficients using the curve-fitted wake profiles (not presented here, see Siauw (2008), for details) show that there is a slight decrease followed by a gradual increase. The decrease in C_d is due to a decrease in the size of the wake between $t^+ = 11.8$ and 13.6. This is significantly different from the jet deployment process, during which there is a rapid increase in C_d before it reduces to its asymptotic level with a lower C_d compared to the uncontrolled state.

4.2. POD analysis

First we analyze the time instant at $t^+ = 0.464$ when the wake has not yet been influenced by the deployment of the FVGs. This will serve as a reference for the dynamical system analysis. Fig. 8 reveals the length scales associated with vortex shedding in the wake for the first and second modes of the POD. A length scale corresponding to $0.18c$ and $0.36c$ can be determined from the first and second modes, respectively.

For the transient dynamics study, the modes are constructed with respect to the initial state of the flow ($t^+ = 0.464$). Thus, the spatial modes are interpreted as changes with respect to the conditional averaged velocity field at $t^+ = 0.464$ and not interpreted in the usual sense of a turbulent fluctuation. As shown in Fig. 9, there is a rapid convergence of the cumulative POD eigenvalues,

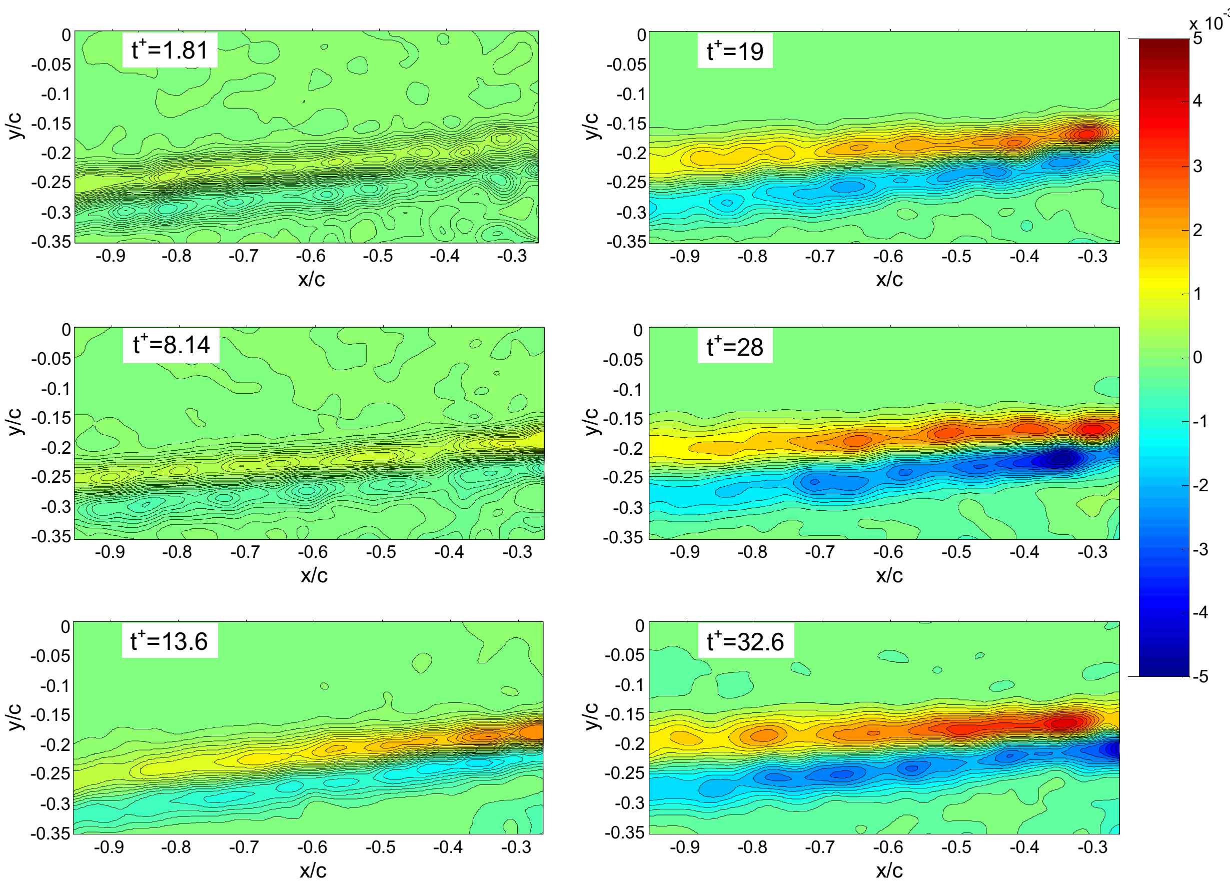

Fig. 7. Evolution of the ensemble-averaged turbulent shear stress ($\langle u'v'\rangle/U_\infty^2$) in the airfoil wake during the separation process.

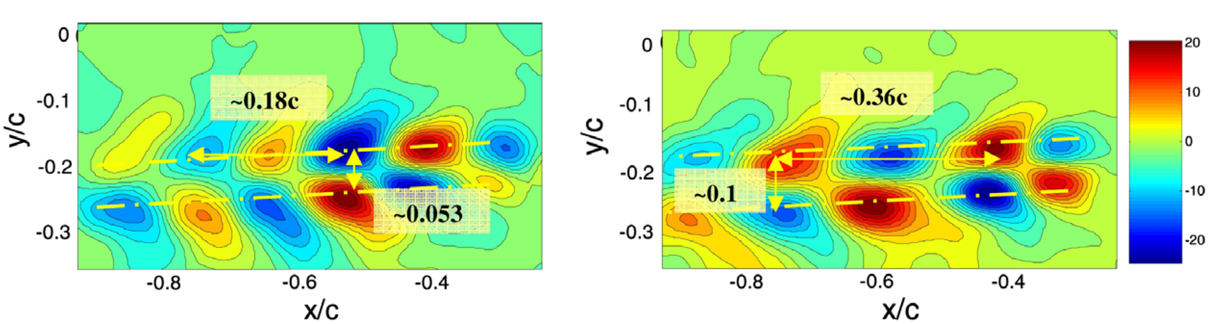

(a) Mode 1. (b) Mode 2.

Fig. 8. Two first POD modes (u-component) for the uncontrolled configuration.

the so-called relative information content (see Cordier and Bergmann, 2008a) for the attachment and separation processes. Indeed, four modes are sufficient to capture 98% of the flow transient energy during jet deployment (Fig. 9a) and 99% of the energy during jet removal (Fig. 9b). The POD ROM will then be identified for the first four modes. The corresponding spatial POD modes are shown in Fig. 10 for the FVGs deployment. Spatial mode 1 corresponds to the mode that is responsible for the change in state from a larger wake to a smaller wake. It can be viewed as the dominant mode that modifies the momentum distribution in the region of the uncontrolled wake axis into that of the controlled wake. In the process, the size and position of the wake axis will be modified. Mode 2, which manifests itself as a large eddy, could be interpreted as the mode that causes the flow to displace slightly upwards before directing the flow downwards. Mode 3 is interpreted as the distortion of the conditional averaged velocity field due to the passage of large eddies. The reader is referred to Siauw (2008) for the spatial POD modes for the jet removal process.

Four modes have been used to model the transient processes. The temporal POD modes $a_i(t)$ $(i = 1–4)$ as shown in Fig. 11 for the jet deployment process are substituted into (5). The acceleration term da_i/dt is computed by a first-order finite difference approximation; thus, we have an over-determined set of linear Eqs. (40 linear constraints to determine five variables) for each mode. The coefficients A_{ij} and B_i are then solved by the method of least squares. The control command $b(t)$, measured by a hotwire at the exit of the jet orifice, has been used with a time delay associated with the convection time for the signal to reach the PIV window. This time delay is approximated by taking the total distance from the position of the orifice to the mid position of the PIV window and considering a convection velocity inferred by a cross-correlation analysis (Siauw, 2008). The time delay is equivalent in non-dimensional units to $t^+ = 4.76$. The identified model (5) is then integrated in time over a period equal to 40 (in plus units) with zero initial conditions. In comparison, the period of actuation corresponds roughly to five times the period of integration of the model. As shown in Fig. 11, the modeled temporal modes $a_i(t)$, determined by integration of (5), and those obtained from POD are in close agreement for all the POD modes. Clearly, the first temporal POD mode (Fig. 11a) describes a change between two states (jet activated and deactivated states) justifying *a posteriori* the use of a first-order system for the model (5). Here, the corresponding time-constant is determined as the time instant when the variable reaches 90% of the asymptotic value. Keeping in mind the value of the time delay, a typical time $t^+ \sim 10$ can be attributed to the jet activation process. The second POD mode, which peaks at $t^+ = 10.2$, describes the movement of a virtual large eddy (2nd spatial mode) that starts to appear at about $t^+ = 6.69$ and diminishes to a small but constant value at $t^+ = 15$. For the jet removal process, a similar good agreement is found between the identified model and the original POD dynamics (Siauw, 2008), with only larger deviations for the fourth POD mode. In this case, a time-constant approximately equal to $t^+ = 20$ is determined to complete

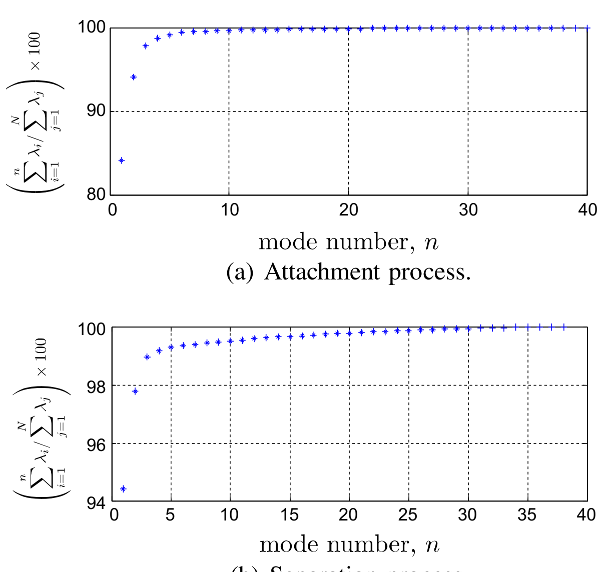

(a) Attachment process.

(b) Separation process.

Fig. 9. Convergence of the POD modes for the attachment and separation processes. λ_i corresponds to the ith POD eigenvalue.

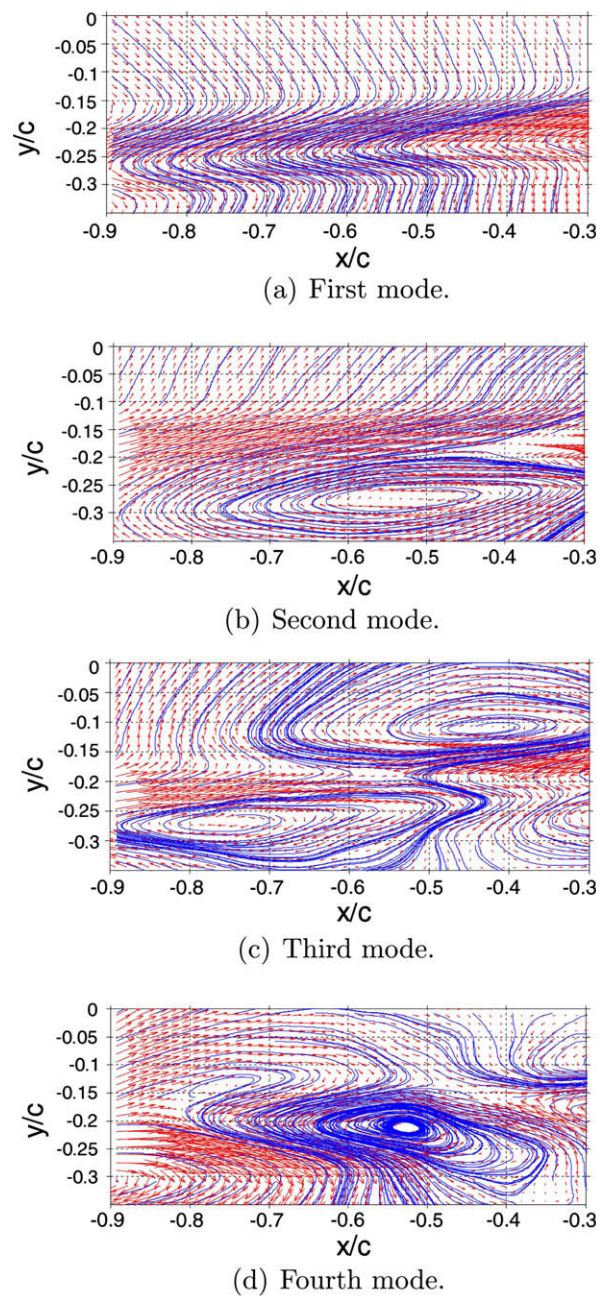

(a) First mode.

(b) Second mode.

(c) Third mode.

(d) Fourth mode.

Fig. 10. Plot of the in-plane streamlines (blue) and vector plot (red) of spatial modes from the conditional POD for the jet deployment process. (For interpretation of the references to colour in this figure legend, the reader is referred to the web version of this article.)

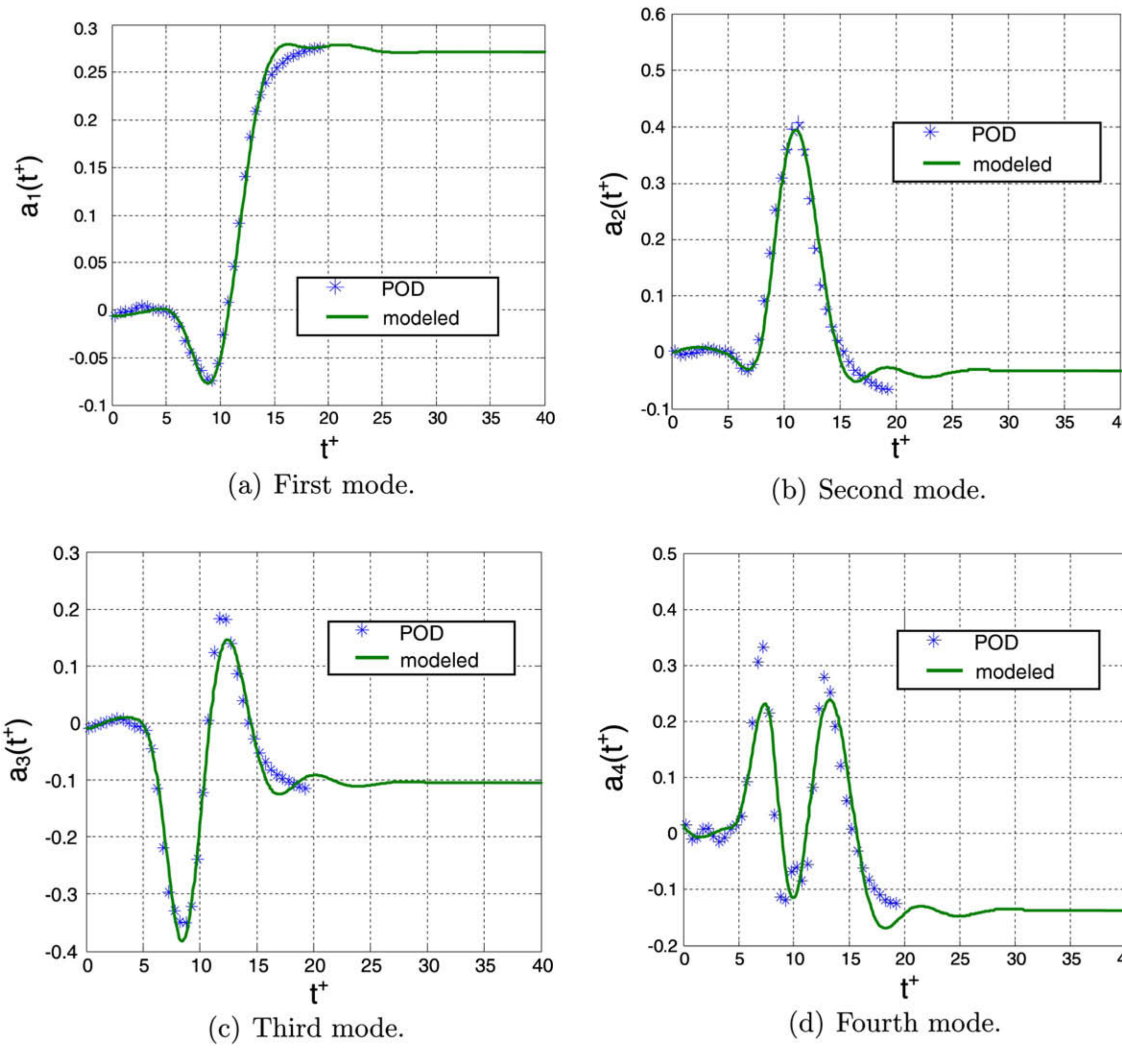

(a) First mode.

(b) Second mode.

(c) Third mode.

(d) Fourth mode.

Fig. 11. Plot of the temporal modes from the conditional POD for the jet deployment process compared to the modeled coefficients using a first order response function. The period of "on–off" actuation is approximately equal to 381 (in plus units). (For interpretation of the references to colour in this figure legend, the reader is referred to the web version of this article.)

the change in state of the first mode. This is twice the value found in the deployment case. The second mode describes the initial downward movement of the wake before moving back upwards. This can be observed by analyzing the ensemble-averaged mean spanwise velocity in the wake axis region (see Siauw, 2008). The contour level at the wake axis becomes more negative (from $t^+ = 4.52$ to 13.6) before assuming less negative values (from $t^+ = 13.6$ to 36.2). Clear similarities are observed in the first and second modes (both spatial and temporal) when compared with the jet deployment case. Thus, the transient dynamics for these two different flow control processes, both of which describe a change between two states, are similar when t^+ are scaled by the respective time intervals for the transient processes.

5. Concluding remarks

The transient dynamics of attachment and separation over a NACA 0015 airfoil at high Reynolds number were studied in response to activation and deactivation of an array of fluidic vortex generators. The flow of the near wake is analyzed via conditional PIV measurements. The attachment process shows a strong transient effect associated with the passage of a starting vortex see (Siauw, 2008) for the determination and analysis of the spanwise vorticity. On the other hand, when the FVGs are deactivated, a more progressive separation process is observed. In the current work, conditional POD analysis of ensemble-averaged PIV velocity fields is used to determine the time scales of the attachment and separation processes. A rapid POD convergence is obtained in both processes, requiring only four POD modes to capture at least 98% of the flow transient energy. Analysis of the first temporal POD mode provides estimates of the typical dimensionless time scale for attachment of $t^+ \sim 10$. It should be noted that this value is in agreement with the airfoil experiment of Amitay and Glezer (2002a), but less comparable with the ramp results of Darabi and Wygnanski (2004a). The discrepancy with the second reference can be attributed both to Reynolds number and geometric effects. In contrast, the time interval for separation ($t^+ \sim 20$) when the jets are deactivated lies within the results presented in Table 1, suggesting this time scale is approximately independent of actuator dynamics, geometry, and Reynolds number.

Clearly, the presented open-loop model can be used for exploration and closed-loop control design. In fact, this closed-loop design with an initially open-loop model has been exercised in a couple of experiments by the authors (Pastoor et al., 2008, 2006).

Acknowledgements

B.R.N. thanks for funding from CNRS (invited researchers grant) and the DFG (Deutsche Forschungsgemeinschaft). The contribution of L.C. to this work was supported by l'Agence Nationale de la Recherche under the CORMORED project ANR-08-BLAN-0115.

References

Adrian, R.J., 1996. Stochastic estimation of the structure of turbulent fields. Eddy Structure Identification, Vol. 145. J.-P. Bonnet.

Allan, B.G., Juang, J.-N., Raney, D.L., Seifert, A., Pack, L.G., Brown, D.E., 2000. Closed-loop separation control using oscillatory flow excitation. Technical report, ICASE-2000-32, Langley Research Center.

Amitay, M., Glezer, A., 2002a. Controlled transient of flow reattachment over stalled airfoils. Int. J. Heat Fluid Fl. 23, 690–699.

Amitay, M., Glezer, A., 2002b. Role of actuation frequency in controlled flow reattachment over a stalled airfoil. AIAA J. 40 (2), 209–216.

Amitay, M., Glezer, A., 2006. Flow transients induced on a 2D airfoil by pulse-modulated actuation. Exp. Fluids 40, 329–331.

Ausseur, J.M., Pinier, J.T., Glauser, M.N., 2006a. Flow separation control using a convective based POD approach. AIAA paper 2006–3017.

Ausseur, J.M., Pinier, J.T., Glauser, M.N., Higuchi, H., 2006b. Experimental development of a reduced order model for flow separation control. AIAA paper 2006–1251.

Bendat, J.S., Piersol, A.G., 1971. Random Data: Analysis and Measurement Procedures. Wiley Interscience.

Bergmann, M., Cordier, L., 2008. Optimal control of the cylinder wake in the laminar regime by trust-region methods and POD reduced order models. J. Comp. Phys. 227, 7813–7840.

Bergmann, M., Cordier, L., Brancher, J.-P., 2005. Optimal rotary control of the cylinder wake using POD reduced order model. Phys. Fluids 17 (9), 097101:1–097101:21.

Burl, J.B., 1999. Linear Optimal Control: H_2 and H_∞ Methods. Addison-Wesley Publishing.

Collis, S.S., Joslin, R.D., Seifert, A., Theofilis, V., 2004. Issues in active flow control: theory, control, simulation, and experiment. Prog. Aerospace Sci. 40, 237–289.

Cordier, L., Abou El Majd, B., Favier, J., 2010. Calibration of POD reduced-order models using Tikhonov regularization. Int. J. Numer. Meth. Fluids 63 (2).

Cordier, L., Bergmann, M., 2008a. Proper orthogonal decomposition: an overview. In: Lecture Series 2002-04, 2003-03 and 2008-01 on Post-Processing of Experimental and Numerical Data. Von Kármán Institute for Fluid Dynamics.

Cordier, L., Bergmann, M., 2008b. Two typical applications of POD: coherent structures eduction and reduced order modelling. In: Lecture Series 2002-04, 2003-03 and 2008-01 on Post-Processing of Experimental and Numerical Data. Von Kármán Institute for Fluid Dynamics.

Darabi, A., Wygnanski, I., 2004a. Active management of naturally separated flow over a solid surface. Part 1. The forced reattachment process. J. Fluid Mech. 510, 105–129.

Darabi, A., Wygnanski, I., 2004b. Active management of naturally separated flow over a solid surface. Part 2. The separation process. J. Fluid Mech. 510, 131–144.

Eldredge, R., Bons, J., 2004. Active Control of a Separating Boundary Layer with Steady Vortex Generating Jets. Detailed Flow Measurements. AIAA paper 2004-751.

Erm, L.P., 2001. Parametric study of jet/vortex interactions in AMRL water tunnel. Technical report, DSTO-TR-1209, Defense Science and Technology.

Greenblatt, D., Wygnanski, I.J., 2000. The control of flow separation by periodic excitation. Progress in Aerospace Sciences 36 (7), 487–545.

Haller, G., 2004. Exact theory of unsteady separation for two-dimensional flows. J. Fluid Mech. 512, 257–311.

Hansen, L., Bons, J., 2006. Flow measurements of vortex generator jets in separating boundary layer. J. Propul. Power 2 (3), 558–565.

Holmes, P.J., Lumley, J.-L., Berkooz, G., Mattingly, J.C., Wittenberg, R.W., 1997. Low-dimensional models of coherent structures in turbulence. Phys. Rep. 287, 337–384.

Johnston, J.P., Compton, D.C., 1992. Streamwise vortex production by pitched and skewed jets in a turbulent boundary layer. AIAA J. 30 (3), 640–647.

Kostas, J., Soria, J., Chong, M.S., 2005. A comparison between snapshot POD analysis of PIV velocity and vorticity data. Exp. Fluids 38, 146–160.

Luchtenburg, D.M., Guenther, B., Noack, B.R., King, R., Tadmor, G., 2009. A generalized mean-field model of the natural and high-frequency actuated flow around a high-lift configuration. J. Fluid Mech. 623, 283–316.

Lumley, J.L., 1967. Atmospheric turbulence and wave propagation. In: The structure of inhomogeneous turbulence. Nauka, Moscow, pp. 166–178.

Mathis, R., Lebedev, A., Collin, E., Delville, J., Bonnet, J.-P., 2009. Experimental study of transient forced turbulent separation and reattachment on a bevelled trailing edge. Exp. Fluids 46 (1), 131–146.

Pastoor, M., Henning, L., Noack, B.R., King, R., Tadmor, G., 2008. Feedback shear layer control for bluff body drag reduction. J. Fluid Mech. 608, 161–196.

Pastoor, M., Noack, B.R., King, R., Tadmor, G., 2006. Spatiotemporal waveform observers and feedback in shear layer control. In: 44th AIAA Aerospace Sciences Meeting and Exhibit. Reno, Nevada, USA, 9–12 January 2006, AIAA-Paper 2006-1402.

Perret, L., Collin, E., Delville, J., 2006. Polynomial identification of POD based low-order dynamical system. J. Turbul. 7, 1–15.

Pinier, J.T., Ausseur, J.M., Glauser, M.N., Higuchi, H., 2007. Proportional closed-loop feedback control of flow separation. AIAA J. 45 (1), 181–190.

Rapoport, D., Fono, I., Cohen, K., Seifert, A., 2003. Closed-loop vectoring control of a turbulent jet using periodic excitation. J. Propul. Power 19 (4), 646–654.

Reynolds, W.C., Hussain, A.K.M.F., 1972. The mechanics of an organized wave in turbulent shear flow. Part 3. Theoretical models and comparisons with experiments. J. Fluid Mech. 54 (2), 263–288.

Seifert, A., Greenblatt, D., Wygnanski, I., 2004. Active separation control: an overview of reynolds and mach numbers effects. Aerosp. Sci. Technol. 8, 569–582.

Siauw, W.L., 2008. Transient process of separation and attachment over a NACA 0015 airfoil controlled by fluidic vortex generators. Thèse de doctorat. University of Poitiers, France.

Sondergaard, R., Rivir, R.B., Bons, J.P., 2002. Control of low-pressure turbine separation using vortex generators. J. Propul. Power 18 (4), 889–895.

Stalnov, O., Palei, V., Fono, I., Cohen, K., Seifert, A., 2007. Experimental estimation of a D-shaped cylinder wake using body mounted sensors. Exp. Fluids 42, 531–542.

Stanislas, M., Okamoto, K., Käehler, C., Westerweel, J., Scarano, F., 2008. Main results of the third international PIV challenge. Exp. Fluids 45 (1), 27–71.

Tadmor, G., Lehmann, O., Noack, B.R., Morzyński, M., in press. Mean field Galerkin models for the natural and actuated cylinder wake flow. Phys. Fluids.

Tian, Y., Song, Q., Cattafesta, L., 2006. Adaptive Feedback Control of Flow Separation. AIAA paper 2006-3016.